International Journal of Peptide Research and Therapeutics (2022) 28:65
https://doi.org/10.1007/s10989-022-10373-6

Modeling Substrate Coordination to Zn-Bound Angiotensin Converting Enzyme 2

Peter R. Fatouros[1] · Urmi Roy[2] · Shantanu Sur[3]

Accepted: 27 January 2022 / Published online: 9 February 2022

Abstract
The Angiotensin Converting Enzyme 2 (ACE2) is a crucial regulator for the renin-angiotensin system. ACE2 converts the Angiotensin (Ang) II peptide into Ang 1–7 and thus promotes various anti-proliferative, anti-inflammatory and cardioprotective effects. In this study, we computationally designed several Ang II mutants to find a strong binding sequence to ACE2 receptor and examined the role of ligand substitution in the docking of native as well as mutant Ang II to the receptor. The peptide in the ACE2-peptide complex was coordinated to zinc (Zn) in the ACE2 cleft. The MD-generated root-mean-square deviation values were mostly similar between the native and mutant peptides considered in this work. The initial peptide-ACE2 poses were generated by molecular docking. The MD simulations used were post-processed by MM-PBSA to generate the binding free energies. All of the peptides studied here demonstrated negative binding free energies, which suggest that all the tested peptides form stable complexes with ACE2. Additionally, by examining the trends in the binding free energies calculated with different internal dielectric constants, it is evident that native Ang II and two of its variants have strongest binding to ACE2 receptor. Even though free energy measurements through classical MD simulation have certain limitations, in the absence of the availability of crystal structures of ACE2-peptide complexes, our work provides some structural insights for various Ang II analogs and how they may interact with a zinc atom within the active site of the enzyme.

Keywords Angiotensin II · Angiotensin converting enzyme 2 · Binding free energy · Metalloenzyme · Molecular dynamics simulation · Zinc parameterization

Introduction

A key regulator for the renin-angiotensin system (RAS) is Angiotensin Converting Enzyme 2 (ACE2). ACE2 has multiple functions including but not limited to controlling hypertension and cardiovascular diseases, and very recently, ACE2 has been identified as a receptor for highly pathogenic SARS-CoV-2. The Angiotensin (Ang) II peptide is converted into Ang 1–7 by ACE2, and thus promotes hemodynamic regulatory and cardio protective effects through various mechanisms including vasodilation, anti-proliferative, and anti-inflammatory activities (Burrell et al. 2004; Santos 2014).

Physiologically, ACE2 cleaves a single amino acid from the C-terminus of the octapeptide Ang II to regulate blood pressure. ACE2 can be classified as a gluzincin from the amino acid sequence found coordinating to zinc at the Ang II binding site. Based on the known properties of the metalloprotease in this class, such a catalytic process would occur through nucleophilic addition of a water molecule coordinated to zinc found within the ACE2 structure (Towler et al. 2004; Cerdà-Costa and Gomis-Rüth 2014).

The COVID-19 pandemic caused by SARS-CoV-2 has emerged as a major health issue with global impacts higher than any other infectious disease in recent history (Padhan and Prabheesh 2021). One major challenge in containing the spread of the disease stems from a high level of respiratory

✉ Urmi Roy
urmi@clarkson.edu

✉ Shantanu Sur
ssur@clarkson.edu

[1] Department of Chemical and Biomolecular Engineering, Clarkson University, 8 Clarkson Avenue, Potsdam, NY 13699, USA

[2] Department of Chemistry and Biomolecular Science, Clarkson University, 8 Clarkson Avenue, Potsdam, NY 13699, USA

[3] Department of Biology, Clarkson University, 8 Clarkson Avenue, Potsdam, NY 13699, USA

transmission. Decreasing the ability of the virus to infect the respiratory epithelial cells could offer an effective measure to control disease spread and severity. To infect hosts' cells, spike (S) protein found in SARS-CoV-2 will first be primed by the transmembrane serine protease 2 (TMPRSS2), acting on the S2 domain (Glowacka et al. 2011; Shulla et al. 2011) The S1 domain of the primed S protein, displayed on the virus surface, will then interact with ACE2 receptor located in the lipid rafts of hosts' cell membranes, inducing endocytosis and eventual infection (Li et al. 2003; Jia 2016). To prevent the viral infection, several research groups have aimed to block this interaction by inhibiting the S protein. This approach requires robust structural studies as well as the design of novel inhibitors with high affinity for the S protein. Additionally, molecular dynamics (MD) simulations were used to study the ACE2-S protein interactions (Ali and Vijayan 2020; Amin et al. 2020; Ghorbani et al. 2020; Han and Král 2020; Spinello et al. 2020; Williams-Noonan et al. 2021; Kuznetsov et al. 2022).

Alternatively, inhibitors can be developed for ACE2 utilizing its native substrate, angiotensin II (Ang II) peptide as a starting structure. The success of such approach will highly depend on the affinity of Ang II for ACE2. And the affinity can potentially be further improved through alterations in the Ang II primary structure, as shown in the study by Clayton et al. (Clayton et al. 2015). Although Clayton et al. have experimentally screened a number of mutant Ang II sequences, several other sequence possibilities are yet to be examined. With the goal of finding a peptide that binds strongly to the ACE2 receptor, we have used computational methods to determine and compare the affinities of reported and additional unexamined Ang II mutants.

Although it is estimated that 10% of the human proteome contains zinc, it remains challenging to completely parameterize it for MD simulations (Andreini et al. 2006). Interactions between zinc and amino acids (cysteine, histidine, tyrosine, and carboxylic acids) can be unusually strong and can involve complex charge transfer and polarization, which are not accounted for in classical Amber or CHARMM force field parameters (Gresh 1995; Lin and Lim 2004; Calimet and Simonson 2006; Li et al. 2008; Trzaskowski et al. 2008). While several methods have been developed to parameterize these interactions, these strategies generally fall into two main categories, namely bonded and non-bonded models. The bonded model generates explicit bonds between zinc and coordinating atoms, fixing the coordination geometry and preventing ligand exchange (Vedani and Huhta 1990; Hoops et al. 1991; Toba et al. 1999). This method also involves the calculation and assignment of partial charge on the zinc ion, which is more realistic than assignment of the formal + 2 charge (Bredenberg and Nilsson 2001; Lin and Wang 2010; Peters et al. 2010). In contrast, the non-bonded model assigns a + 2 integer charge on zinc and allows for ligand exchange during MD simulations (Stote and Karplus 1995). However, this model is not suitable to describe the tetra- and penta-coordinated structures and tends to prefer octahedral coordination geometries (Hoops et al. 1991; Donini and Kollman 2000; Koca et al. 2003; Zhang et al. 2012).

Computational approaches are commonly used in drug design as they allow for reductions in cost and time when scanning for new targeting molecules. In these approaches, potential inhibitors or active substrates are docked to the receptor and undergo molecular dynamics (MD) simulations followed by calculations of binding free energy. These provide the ability to accurately estimate the interactions that could be further experimentally validated, which critically depends on the assignment of proper parameters to all atoms and interactions found within the system for the MD simulations and calculations.

In this work, we design, dock, and simulate several Ang II mutant sequences to find a strong binding sequence for ACE2. Native peptide and each mutant were docked to zinc at each of the possible coordination sites found within the peptide, replacing the existing water molecule at the coordination site. Additionally, we briefly examine the potential impact of peptide binding to ACE2 on the structure of the SARS-CoV-2 spike (S) protein binding region on ACE2.

Materials and Methods

Obtaining Structures

The experimentally derived structures for Ang II and ACE2, 1N9V (Spyroulias et al. 2003) and 1R42 (Towler et al. 2004) respectively, were obtained from the RCSB PDB (rcsb.org) (Berman et al. 2000). Initial Ang II mutants' structures were derived through use of PDB manipulator (Jo et al. 2014) found in CHARMM-GUI (Jo et al. 2008; Brooks et al. 2009; Lee et al. 2016) to induce single-point mutations. To improve these structures, Visual Molecular Dynamics (VMD) (Humphrey et al. 1996) was used to add a water box with a padding of 5 Å as well as add Na^+ and Cl^- ions to neutralize charge and establish a NaCl concentration of 0.15 M. The mutants then underwent minimization under constant temperature (310 K) and pressure (1 atm) for 10,000 iterations with a step size of 1 fs using Nanoscale Molecular Dynamics (NAMD) (Phillips et al. 2005). This simulation includes the use of Particle mesh Ewald (PME) method to account for electrostatic interactions with a manual grid definition based on rounded periodic boundary conditions. Temperature is controlled through Langevin dynamics with a damping coefficient of 5 ps^{-1} applied to non-hydrogen atoms. Pressure was controlled through use of a Langevin piston set to 1.01 bar, with an oscillation period of 100 fs and a

damping timescale of 50 fs. All bonds to hydrogen are constrained using the ShakeH algorithm. Before proceeding, Ramachandran plots created with MolProbity (Chen et al. 2010) and RMSD plots created in VMD were analyzed to check the generated structures and the minimization procedure. It was found that 10,000 iterations were sufficient to allow the proteins' backbones to reach a constant RMSD, and for total energy, as observed in the NAMD output file, to converge to a minimum value.

Docking and Model Selection

To dock the desired ligands from Ang II or mutant peptides to zinc within the ACE2 structure, GM-DockZn (Wang et al. 2020) was used. This program determines potential coordination sites on the ligand molecule and docks each site to the zinc ion. While models are typically sorted with a scoring function, in this scenario, models are preferably selected based on coordination geometry. It is critical that the coordination geometry is made accurate during docking, as it will become fixed during zinc parameterization using the bonded model. As previously demonstrated by Der, ideal coordination distances and angles involving zinc were used to score each docked model's coordination geometry (Der 2013). The values used for model evaluation are included in Table S1 in the Supplementary Information 1 (SI 1). Using these scores, four structures were selected for each peptide sequence, coordinated to zinc at first, fourth, sixth, and C-terminal residue of the sequence.

Zinc Parameterization

To prepare structures for parameterization, structural files were first converted from CHARMM to Amber format with Bio3D (Grant et al. 2006) which includes the removal of all hydrogen atoms. The protonation state of each titratable residue was determined through version 3.2 of H++, and hydrogens were added accordingly (Gordon et al. 2005; Myers et al. 2006; Anandakrishnan et al. 2012). To parameterize the zinc coordination site, MCPB.py (Li and Merz Jr 2016) was used. The bonded model was selected to reflect partial charges found on the various atoms within the coordination complex and prevent ligand substitution events during later MD simulations. During the MCPB.py procedure, bond and angle parameters for the zinc ion were generated using the Empirical method (Yu et al. 2018). Restrained electrostatic potential (RESP) charges for atoms within the coordination complex were calculated using quantum mechanics (QM) simulations with GAMESS-US (Barca et al. 2020). Using AmberTools20, a water box with a padding of 10 Å and neutralizing Na^+ and Cl^- ions were added (Case et al. 2020).

MD Simulations

Using the solvated and neutralized docked complexes, minimization was performed for 30,000 iterations with a step size of 1 fs at 310 K and 1 atm. The same PME (using new periodic boundary conditions), Langevin dynamics and Langevin piston inputs used in the minimization of peptide structures were used in the minimization of ACE2-peptide complexes. It was found that 30,000 iterations were sufficient to allow the proteins' backbones to reach a constant RMSD, and for total energy, as observed in the NAMD output file, to converge to a minimum value. Equilibration of the docked complexes was then performed at 310 K with constant volume for 2 ns with a step size of 1 fs, followed by a 10 ns production run using the same conditions (Roy 2016, 2019, 2020a, b). Additionally, a 50 ns production run was performed for the native Ang II-ACE2 complexes following equilibration. For these simulations with constant volume, Langevin dynamics settings remained the same as in the minimization protocol while the Langevin piston settings were removed. Additionally, the PME grid was defined using a grid spacing of 1.0 Å instead of using manual grid definition. In all simulations, all bonds to hydrogens were constrained through the ShakeH algorithm. The calculations for all ACE2-peptide complexes were performed on Clarkson University's ACRES cluster using the *Linux-x86_64-ibverbs-smp* version of NAMD. The lowest energy structures for each of these ACE2-peptide complexes during the production runs were determined by calculating the total energy of protein and zinc through use of the NAMD Energy plug-in in VMD. These structures can be found in a zip folder in SI 2. Additionally, clustering was performed in VMD by using a tcl script written by Babu (2018) with a step size of 0.15 ns and a RMSD cutoff of 1 Å. In this clustering protocol, frames from the simulation output with similar conformation (based on a RMSD less than the cutoff value) are grouped together into a cluster. Three clusters were generated for each ACE2-peptide complex with RMSD calculated with respect to the following: the S-protein binding site on ACE2, the peptide, and all ACE2 residues. For each complex, the cluster that contains the most frames is called the highest frequency structure. The cluster center of the highest frequency cluster for each ACE2-peptide complex has been included in a zip file found in SI 3. For the native and mutant Ang II peptides alone, production runs of 48 ns were performed, after 2 ns equilibration (using the same constant volume NAMD protocol described above). The calculations of these relatively smaller sized systems were performed with a multicore version of NAMD on a Linux server.

Binding Free Energy Calculations

The Molecular Mechanics/Poisson-Boltzmann Surface Area (MM/PBSA) approach was used to determine binding free energies utilizing trajectories created during the MD production runs The CaFE (Liu and Hou 2016) plugin for VMD, which utilizes APBS (Baker et al. 2001), NAMD and VMD, was used to calculate the free energies of the ligand, receptor and docked complex. It is to be noted that binding free energies computed through the MM/PBSA method are sensitive to the internal dielectric constant, and therefore, needs careful selection of this value (Wang et al. 2019). The optimal value for the interior dielectric constant depends on the characteristics of the protein–ligand interface. This is because the highly polar and charged sites require greater internal dielectric constants (Hou et al. 2011). In the ACE2-peptide complexes, the active site contains the charged zinc ion and several other charged and polar residues, suggesting the use of higher internal dielectric constants instead of using the default value of 1 (Adekoya et al. 2006; Rifai et al. 2019). Thus, calculations were performed for internal dielectric constants of 1, 2, 4, 6, and 8 while the solvent dielectric constant for water, which is generally unmodified, was set to the default value of 80. Due to the required number of calculations and the increasing computational costs at greater internal dielectric constants, the binding energy was calculated at 0.15 ns intervals throughout each 10 ns production run. In this protocol, the free energy is computed for the receptor-ligand complex as well as the free ligand and receptor in each frame of the production run trajectory. NAMD is used to calculate the gas phase free energy while APBS and VMD calculate the polar and nonpolar solvation energies, respectively. The binding free energy is computed by subtracting the average free energies of the ligand and receptor from the average free energy of the receptor-ligand complex.

Results

To study the influence of peptide sequence on ACE2 binding, we considered seven mutant Ang II peptides and compared those against the native Ang II sequence (Fig. 1A). The mutant peptides were obtained by making single or double point mutations at amino acid positions 4–6 of the native sequence. The structures of these peptides are included in the SI 1 Fig. S1. The binding affinity between Ang II and ACE2 largely depends on the peptide concentration. Thus, at lower concentrations the native Ang II and two of its mutant sequences (DRVYI**Y**PF and DRVY**VY**PF) exhibited enhanced binding to the angiotensin type 2 (AT_2R) receptor. These two peptides were also demonstrated to increase ACE2 inhibition at relatively higher concentrations (Clayton et al. 2015). The other five mutants were designed to test the replacement of tyrosine (Y) with the stronger coordinating residues, glutamic acid (E) and cysteine (C). The stability of the mutant peptides was analyzed by computing the RMSD over a 48 ns production run (Fig. 1B and Fig. S2). We observed that the average RMSD values and the magnitudes of fluctuations of these mutant peptides (range of average RMSD and standard deviations: 3.96–5.51 ± 0.67–1.10 Å) were marginally lower to the average RMSD value of native Ang II (4.76 ± 0.90 Å). The secondary structure-changes and the Ramachandran plots for each minimized peptide can be found in SI 1 Figs. S3–S4.

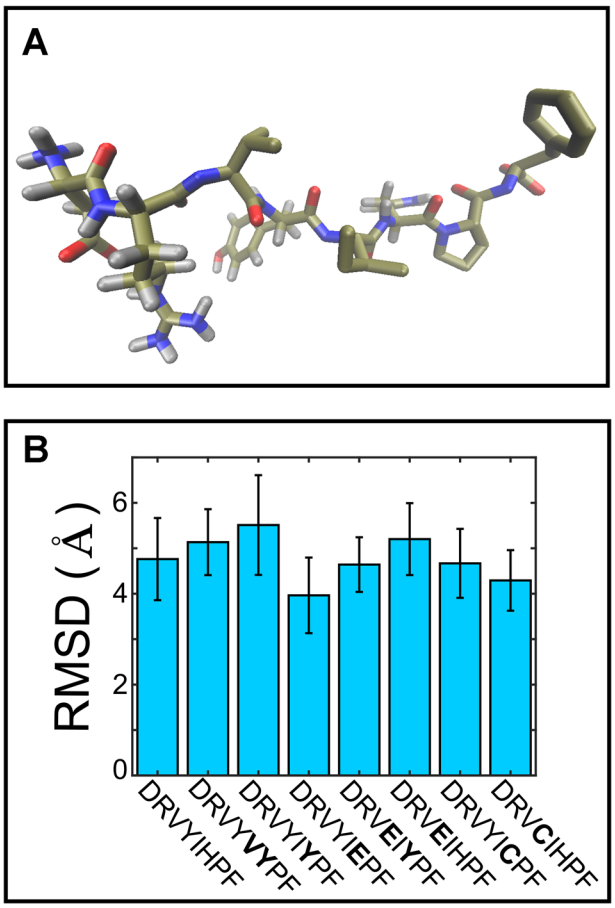

Fig. 1 **A** The minimized and equilibrated structure of Ang II. **B** Averaged RMSD of Ang II and seven Ang II mutants during a 48 ns production run. The bolded residues found in the peptide sequences indicate the mutations from the native Ang II sequence (Color figure online)

Docked ACE2-peptide structures were obtained, where the peptide was coordinated to zinc in the ACE2 cleft as shown in Fig. 2A. To be noted in this context that the SARS-CoV-2 S1 binding region on ACE2, as obtained from literature (Han and Král 2020), is located outside the Ang II binding pocket. From the classification and known activity of ACE2, it is known that the zinc ion found in ACE2

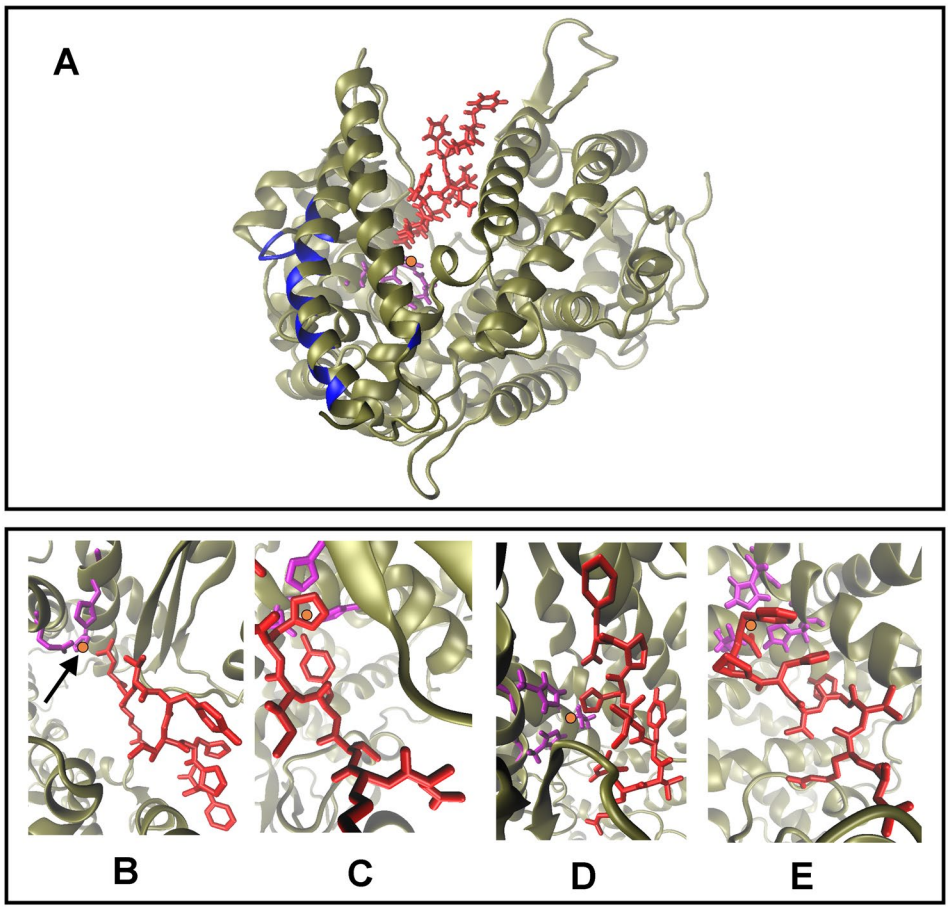

Fig. 2 **A** The structure of Ang II (red) bound to ACE2 (tan). The residues on ACE2 that interact with spike protein are shown in blue. **B–E** Magnified views of Ang II-ACE2 binding, depicting the coordination of Ang II to zinc (orange) at four possible residues of D, Y, H, and the C-terminus, shown in **B**, **C**, **D**, and **E**, respectively. Corresponding coordinating residues on ACE2 are shown in purple (Color figure online)

participates in the cleavage of phenylalanine (F) residue from Ang II (Cerdà-Costa and Gomis-Rüth 2014). When Ang II peptide approaches the zinc ion located in the ACE2 cleft, ligand substitution can occur, with peptide replacing the water typically found coordinating to zinc. Several sites on Ang II can participate in this coordination including aspartic acid (D), tyrosine (Y), histidine (H), and the C-terminus of the peptide. Coordination with zinc at each of these sites can be quite strong, thus allowing a stable binding of the peptides to ACE2 without being cleaved, as was determined experimentally (Clayton et al. 2015). Four complexes were generated for each unique Ang II mutant, with a different residue of the peptide coordinated to zinc in each. Figure 2B–E show the four structures generated for native Ang II, with Ang II coordinated to zinc at residues one (D), four (Y), six (H), and the C-terminus.

Next, we examined the stability of the ACE2-peptide complex and compared the differences due to coordination at various sites of interest within the complex. The RMSD of the ACE2-peptide complexes was calculated throughout the duration of the 10 ns production run (Fig. 3A). To verify that this runtime is sufficient to capture the true behavior, 50 ns production runs were performed for the native Ang II-ACE2 complexes to compare the effects of a longer simulation time (Fig. 3B). We found that the longer simulation time did not make a major impact on the average RMSD or magnitude of fluctuations, thus confirming the validation of the results from a shorter run of 10 ns. The.pdb files of lowest-energy structures for each of the ACE2-peptide complexes during the production run are included in SI 2 for reference. The minimum energy structures of the protein-peptide complex are selected without considering the solvating water molecules or counter ions. These protein-peptide complexes were extracted from the.dcd files of the entire systems. Interestingly, a noticeable difference was observed between the RMSD values of the entire ACE2-peptide complex (Fig. 3A, B) and the peptides within the ACE2-peptide complexes (Fig. 3C, D). The RMSD values of a single peptide demonstrated larger variability when amino acid residues at different positions of the chain were selected to coordinate with zinc. However, the stabilities of zinc coordinated peptides are higher than those of apo-peptides as indicated Figs. 1B and 3. The observed lower RMSD values of Ang II-ACE2 could be attributed to a stabilization induced by zinc coordination, as well as to inter-chain interactions between the peptide and the ACE2 receptor.

The variations in the binding site on ACE2 when native Ang II is coordinated to zinc at different amino acid residues

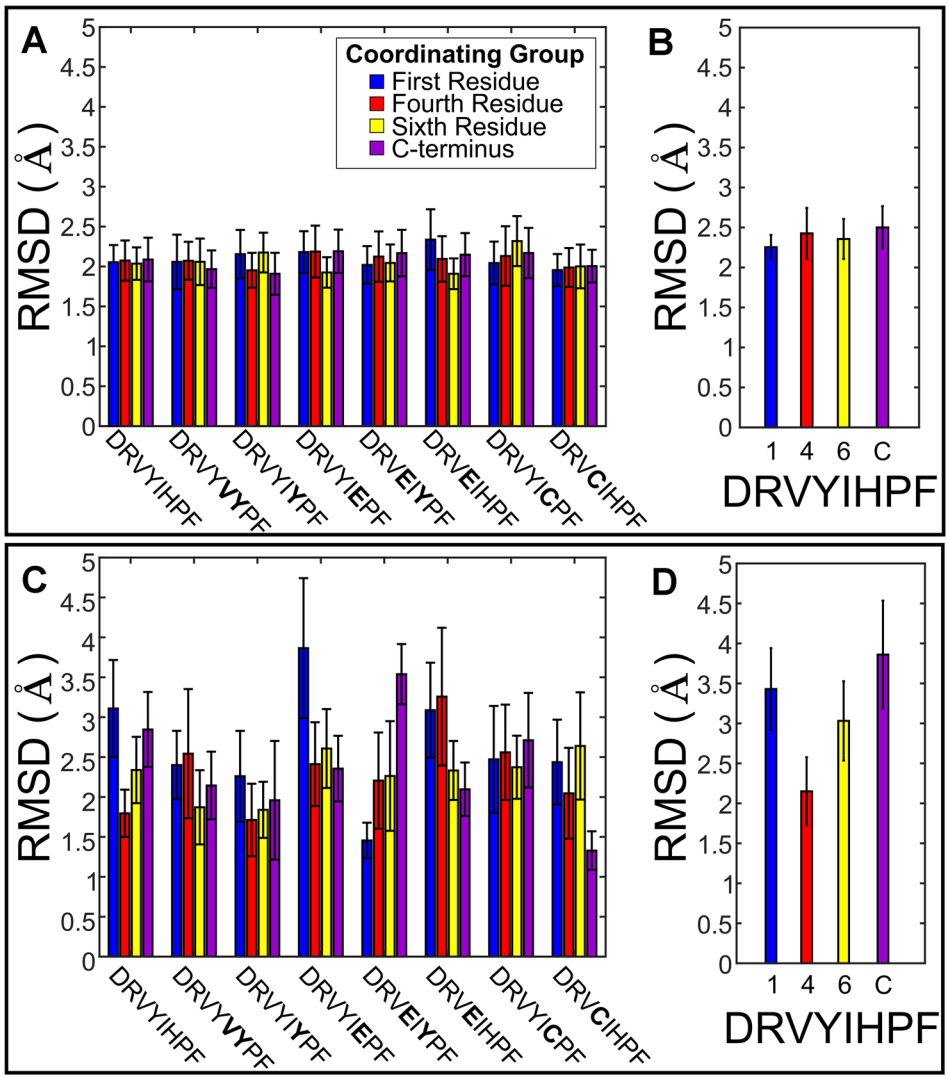

Fig. 3 Computed averaged RMSD values for the entire Ang II-ACE2 protein complexes (**A** and **B**) and just the Ang II peptide or its mutant sequences (**C** and **D**). **A** and **C** correspond to 10 ns production runs while **B** and **D** correspond to 50 ns production runs. Each Ang II mutant has been coordinated to zinc at one of four possible locations on the peptide, as specified by bar color. The bolded residues in the peptide sequence are mutations from Ang II (Color figure online)

are shown in Fig. 4A–D. We found that beyond the movement of peptides during the production run, there were also some structural changes of the peptide binding site on ACE2. The changes in the secondary structure of the interacting residues, namely the residues within 3.5 Å of the peptide in the docked structure of ACE2, during the 10 ns production run are shown in Fig. 4E–H. While the interacting residues with α-helix and β-sheet secondary structures were relatively stable, fluctuations in structures were commonly observed for coils to turns. Furthermore, these changes and disorders were most prominent when the C-terminus of Ang II was coordinated to zinc (Fig. 4H). Previously reported experimental protocols state that C-terminal alterations of peptides tend to impact such secondary structure changes and ligand binding (Clayton et al. 2015). This associated instability of the system is also observed in the RMSD plots of the native peptide (Fig. 3B, D).

The affinity of peptide binding to ACE2 was evaluated by calculation of binding free energy from the ACE2-peptide complexes (Fig. 5). First, we computed binding free energy for each peptide by coordinating zinc to four different positions of the peptide and keeping internal dielectric constant as 1 (Fig. 5). The values of negative ΔG are plotted in Fig. 5. Negative free energies were observed in native Ang II and in all the mutant peptides within the ACE2-peptide complexes. However, we observed unusually high values in native Ang II and DRVY**V**Y**P**F mutant sequence when coordinated to zinc at the fourth residue. We also observed that the DRV**E**I**Y**PF sequence exhibited moderately negative ΔG values when zinc coordination was implemented at the first and fourth (D and E) residues. Interestingly, zinc coordination at the 6th residue showed a relatively low negative ΔG values for the peptides under consideration even when several mutant sequences had residue Y in this position (Fig. 5). Similarly, low negative ΔG was observed when the zinc coordination was performed at the C-terminus of the sequences.

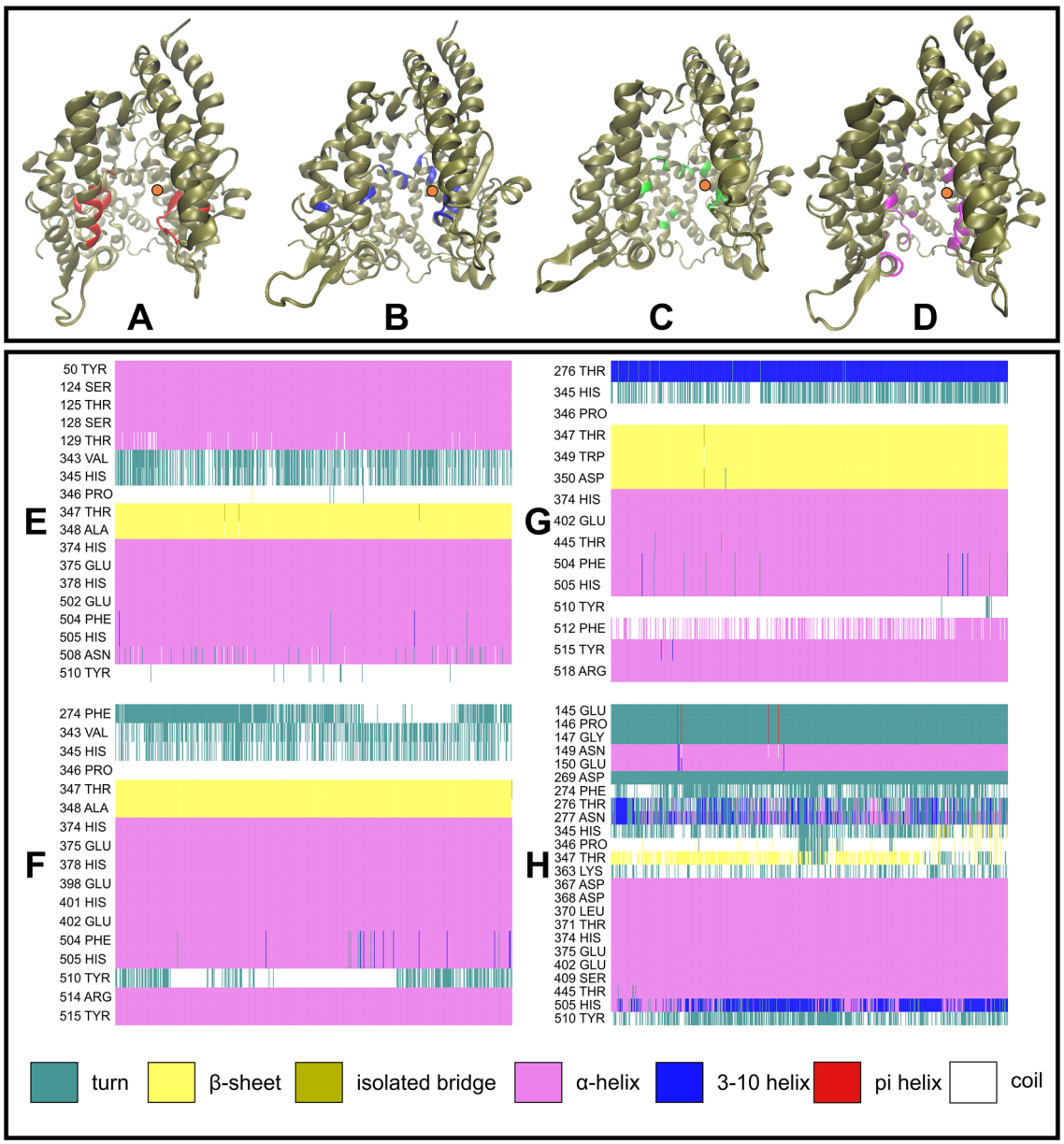

Fig. 4 **A**–**D** ACE2 residues that interact with Ang II when coordinated to zinc at D, Y, H, and C-terminus, respectively. Interacting residues of ACE2 are highlighted with a non-tan color. **E**–**H** Secondary structures of the interacting residues of ACE2 when Ang II is coordinated to zinc at D, Y, H, and C-terminus, respectively, throughout the 10 ns production run (Color figure online)

The charged nature of the ACE2-peptide binding site suggests that consideration of a higher internal dielectric constant in the computation of binding free energy could provide a better estimate. However, experimental binding free energies for ACE2-peptide complexes are not reported in the literature, and without the availability of such data, it is difficult to determine an accurate estimate of internal dielectric constant. Therefore, we additionally computed binding free energies for internal dielectric constants of 2, 4, 6, and 8 (Hou et al. 2011) to examine any trend associated with this change (Fig. 5). Dielectric constants larger than 8 were not used as nearly all binding energies have converged by this point. This approach confirmed our earlier observation that the three peptides with the strongest binding free energies are native Ang II, DRVY**VY**PF, and DRV**EI**YPF. Interestingly, while the binding free energies of both native Ang II and DRVY**VY**PF, coordinated at the fourth residue, are consistently more negative than any other binding free energies, these values are more similar to the other complexes' binding free energies at an internal dielectric constant of 4 and larger (Fig. 5). Additionally, all peptides demonstrated negative free binding energies

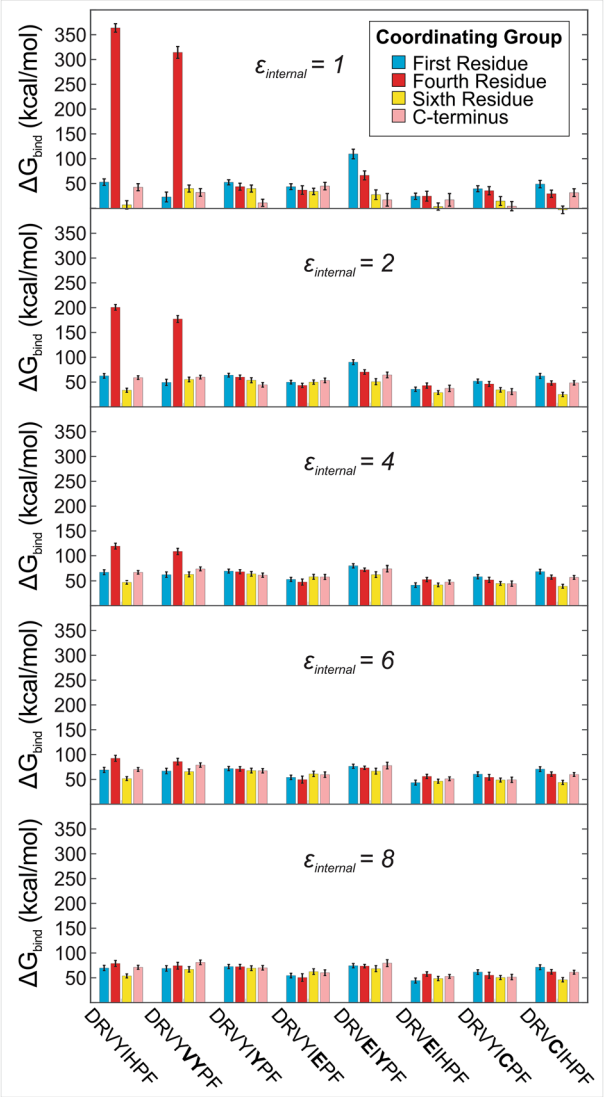

Fig. 5 Binding free energies for the ACE2-peptide protein complexes computed through the MM/PBSA method using internal dielectric constants of 1, 2, 4, 6, or 8 as specified within each graph. The bar color corresponds to the location within the peptide that is coordinated to zinc. Mutations from the native Ang II sequence are bolded. All the values on the vertical axis represent negative numbers (Color figure online)

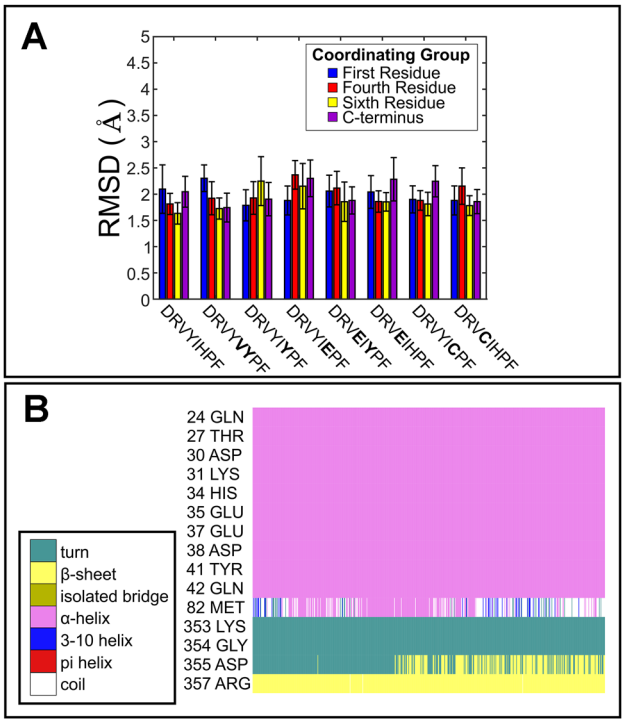

Fig. 6 **A** Averaged RMSD of the S1 binding region on ACE2 during the production run of the various complexes with native Ang II and mutant sequences (mutations are shown in bold font). Each bar color represents a different residue location in the peptide chain coordinating to zinc in the complex. **B** Secondary structures of ACE2 residues that interact with spike protein throughout a 10 ns production run of Ang II-ACE2 complex with native Ang II coordinating to zinc at D. The box to the left explains how colors in the timeline plot correspond to secondary structure features (Color figure online)

at higher internal dielectric constants, which are likely more realistic, suggesting the formation of stable complexes with ACE2.

Finally, we examined whether the interaction of Ang II or the mutant peptides could potentially elicit allosteric inhibition of S1 binding to ACE2 (Fig. 6). The RMSDs of ACE2 residues at the S1 binding region, as identified by Han et al. (Han and Král 2020), were calculated during the production run of the ACE2-peptide complexes (Fig. 6A). The average RMSD values in this figure were comparable to those of the entire protein during this simulation (Fig. 3).

Additionally, we studied the change in secondary structure of the interacting residues located at the S1 binding region during 10 ns production run (Fig. 6B). While the α-helical structure remained stable during the run, some variability in the secondary structure at residues 82 M and 355D were observed. However, this change is unlikely to impact the binding of spike protein to ACE2.

Discussion

The production run for the ACE2-peptide complexes generated higher average RMSD and standard deviation values for the peptides alone when compared with the entire ACE2-peptide complexes (Fig. 3). The higher RMSD values were also observed in the apo-peptides (SI 1 Fig. S2). These different RMSDs can be attributed to the lack of strong secondary structure in the short peptides allowing for greater flexibility and movement than the larger and more structured ACE2 protein. Additionally, it is possible that zinc coordination played a key role in stabilizing these peptides within

the complex and peptide bound complexes. It is not obvious whether and how the zinc was included in previously reported work. Our results also indicate that docking the peptides to ACE2 results in changes in the ACE2 secondary structure (Fig. 4). While residues 274F, 343 V, 345H, 363L and 510Y tend to alternate between the unstable turn and coil configurations in the native Ang II-ACE2 complexes, residues 129 T and 512F become more stable as they shift from turns and coils to various helices and β-sheets.

The initial selection of mutants for this study was based on the experimental work which examined the selectivity of native and mutant Ang II peptides towards various receptors including AT_1R, AT_2R and ACE2 (Clayton et al. 2015). The native and the mutant peptides DRVYI**Y**PF, and DRVY**VY**PF were shown to exhibit a stronger binding towards AT_2R at lower substrate concentration while stronger inhibitions of ACE2 were identified at relatively higher strengths. The results from this experimental work also suggest that the 6th residue of Ang II may play an important role in binding to ACE2. To further understand the role of amino acid residue located at this position, in this work, we investigated three additional mutant sequences DRVYI**E**PF, DRVYI**C**PF and DRV**EI**YPF. Specifically, we examined mutations with introduction of glutamic acid (E) and cysteine (C) as the 6th residue since these amino acids are known to coordinate strongly to the zinc ion. Additionally, in our preliminary analysis on binding energy calculation of native Ang II and DRVY**VY**PF, it was observed that coordination to Y at the 4th position resulted in strong binding to ACE2. To explore the potential role of 4th residue in the binding event, we considered additional sequences with mutations at the fourth position (DRV**EI**YPF, DRV**E**IHPF, and DRV**C**IHPF).

Although experimental finding demonstrated the potential of using mutant peptides for stronger binding and inhibition of ACE2, crystal structures of ACE2-peptide complexes are not yet available. In the absence of crystal structures, the lowest-energy structures of the complexes obtained through MD simulation (included in SI 2) can serve as a reasonable substitute for advancement of research in this direction. Furthermore, refinement of the MD structures were done by clustering based on the RMSD values of S-protein binding site, ligand bound pose, the remainder of ACE2 protein, and selecting the highest frequency clusters (included in SI 3).

The negative binding free energy is an established approach to identify a stable biological system and the MM/PBSA is one of the most widely used endpoint methods for calculating free energies. Our analysis showed that native Ang II and mutant DRVY**VY**PF each form a complex to ACE2 with a notably strong negative binding free energy and thus, further validate the previous experimental observations. Here the fourth amino acid residue (Y) of the sequences was found to coordinate with zinc in these situations (Fig. 5). Additionally, the mutant peptide DRV**EI**YPF showed moderately negative ΔG values at first and fourth residues. For other sequences considered, the Y residue at fourth position had demonstrated slightly negative ΔG values. The mutants with zinc coordination at the 6th position did not manifest any major ΔG deviations. However, variants DRVY**VY**PF, DRVYI**Y**PF, DRVYI**E**PF and DRV**EI**YPF at the 6th position coordinated with zinc exhibited smaller changes in ΔG values compared to the native species. The reasons for the very strong negative binding free energies in the first two cases shown in Fig. 5 are not clearly understood at this time. One potential limitation and a source of variability could be from the lack of entropy calculations in MM/PBSA protocol. However, its impact tends to be small even with the presence of flexible ligands, and therefore, it is highly unlikely to make a substantial contribution to the differences found in our observations. The potential role of kinetics also cannot be excluded as it plays a critical role in computing large binding free energies. It is possible that while these states are thermodynamically favorable, the kinetics presents a large activation energy barrier, preventing the formation of these final states. The impact of kinetics, which requires more computationally expensive techniques, however, is beyond the scope of the current work.

In this work, we calculated binding free energies for a variety of ACE2-binding peptides, coordinated to zinc at four different locations (Fig. 5). While using internal dielectric constants greater than one, which is recommended for charged interaction sites, all peptides coordinated at each potential site had a negative binding free energy. The calculated negative ΔG values in each case further solidify the argument that all of these peptides form stable complexes with ACE2. Additionally, a consistent trend in the computed binding free energies over increasing internal dielectric constants support that strong binding to ACE2 was provided by native Ang II, DRVY**VY**PF, and DRV**EI**YPF sequences.

It is also useful to note in this context that, the usual free-energy perturbation (FEP) technique is not always ideally suited for the calculation of the electrostatic interactions from the sidechains of a doubly-charged phosphotyrosine (Bradshaw and Waksman 1998). There is evidence in the literature that the decoupled scheme may result in very high negative value of free energy changes (Woo and Roux 2005). Results have also been reported along this line, indicating relatively low (~ 10%) accuracy in the classical MD simulated energies of zinc ion coordinated complex (Brandt et al. 2009). In view of these observations, the MD calculated energies of such zinc coordinated systems may have rather large uncertainties, and the high negative energies observed in the first two cases of Fig. 5 may be linked to multiple factors, which we intend to investigate in the future.

The Ang II peptide does not share an active binding site with spike (S) protein of SARS-CoV-2, and thus might not be effective alone in blocking the binding of S protein

(Towler et al. 2004; Yan et al. 2020). During the production run the S1 binding region of ACE2 generated a similar RMSD to the rest of the protein complex, ruling out any increased movement in this region (Fig. 6A). Additionally, the secondary structure of this binding region remains largely unchanged except for the two residues at 82 M and 355D. Both findings suggest very few structural changes in the S1 binding region in response to Ang II binding. Thus, a relatively little impact on the S1 binding region following ACE2-peptide interaction suggests that these peptides alone are less likely to allosterically inhibit the binding of SARS-CoV-2.

However, identifying a peptide sequence that provides a strong binding at the Ang II binding cleft on ACE2 could still be an important step toward developing novel therapeutic strategies to prevent SARS-CoV-2 infection (Moore et al. 2021). A high-affinity peptide sequence conjugated to a nanostructure (Jeong et al. 2018) will enable binding to the ACE2 proteins displayed on the cell membrane surface and can inhibit the interaction with the virus spike protein by physically blocking the access of the S1 binding domain. The efficacy of such strategy can further be enhanced by using the sequence at a very high density on a nanostructure such as self-assembled peptide nanofibers (Sur et al. 2015), which would allow the additional advantage of multivalent binding (Arsiwala et al. 2019).

The computational results presented in this work indicate that the bindings of native and mutant Ang II peptides to ACE2 results in more rigid peptides along with a reorganization of the secondary structure of the binding residues in ACE2 cleft. Additionally, we observed negative ΔG values for all peptides, with highest negative binding energies for the native Ang II and mutants DRVY**VY**PF and DRV**EIY**PF sequences. Lastly, it was found that Ang II binding to ACE2 may not have a significant effect on the secondary structure of S1 binding residues of ACE2, suggesting that Ang II does not allosterically inhibit S protein-ACE2 interaction.

Conclusions

We have performed molecular docking studies to examine the binding of native Ang II sequence and several mutant variants to ACE2 receptor, considering zinc coordination in the interaction. Based on our data, we can infer that that all zinc coordinated peptides form stable complexes with ACE2. The relatively low binding free energies were observed in native peptide and its mutant variants. However, among these sequences, we found that the native Ang II sequence is optimal for binding to the ACE2 cleft with only two of the mutant sequences demonstrating binding energies of similar amplitude. The importance of choosing an appropriate solute di-electric constant for this computation is also discussed in this context. Further, our analysis of S1 binding region suggests that native and mutant Ang II peptides alone are unlikely to inhibit the interaction between ACE2 and S protein. Though, the knowledge of strong binding sequences for the ACE2 cleft could open the possibility of developing new strategies to prevent virus binding to cells. Specifically, presenting these sequences at a high density on a larger nanostructure could efficiently occupy the available ACE2 receptors on cell surface and physically block further access of the virus spike protein to the receptor binding site.

We hope that the results obtained in this study will provide some structural insights into various Ang II analogs and help to understand how they may interact with a zinc atom within the active site of the enzyme. The binding or inhibition of the native or mutant Ang II to its receptors is inevitably dictated by different constraints and parameters of the system. In our future studies of this system, we hope to explore these latter factors.

Supplementary Information The online version contains supplementary material available at https://doi.org/10.1007/s10989-022-10373-6.

Acknowledgements Some of the computing for this project was performed on the ACRES cluster. We would like to thank Clarkson University and the Office of Information Technology for providing computational resources and support that contributed to these research results. Additional computational resources for this grant were provided by the National Science Foundation under Grant No. 1925596. The authors acknowledge use of the following simulation and visualization software packages: (1) NAMD and (2) VMD: NAMD and VMD, developed by the Theoretical and Computational Biophysics Group in the Beckman Institute for Advanced Science and Technology at the University of Illinois, Urbana-Champaign.

Funding No funding was received for conducting this study.

Declarations

Conflict of interest The authors have no relevant financial or non-financial interests to disclose.

References

Adekoya OA, Willassen NP, Sylte I (2006) Molecular insight into pseudolysin inhibition using the MM-PBSA and LIE methods. J Struct Biol 153(2):129–144

Ali A, Vijayan R (2020) Dynamics of the ACE2-SARS-CoV-2/SARS-CoV spike protein interface reveal unique mechanisms. Sci Rep 10(1):14214

Amin M, Sorour MK, Kasry A (2020) Comparing the binding interactions in the receptor binding domains of SARS-CoV-2 and SARS-CoV. J Phys Chem Lett 11(12):4897–4900

Anandakrishnan R, Aguilar B, Onufriev AV (2012) H++ 3.0: automating p K prediction and the preparation of biomolecular structures for atomistic molecular modeling and simulations. Nucleic Acids Res 40(W1):W537–W541

Andreini C, Banci L, Bertini I, Rosato A (2006) Counting the zinc-proteins encoded in the human genome. J Proteome Res 5(1):196–201

Arsiwala A, Castro A, Frey S, Stathos M, Kane RS (2019) Designing multivalent ligands to control biological interactions: from vaccines and cellular effectors to targeted drug delivery. Chem Asian J 14(2):244–255

Babu KA (2018) Cluster -analysis -using -VMD-TCL. https://anjibabuiitk.github.io/CLUSTER-ANALYSIS-USING-VMD-TCL/. Accessed Jan 2022

Baker NA, Sept D, Joseph S, Holst MJ, McCammon JA (2001) Electrostatics of nanosystems: application to microtubules and the ribosome. Proc Natl Acad Sci USA 98(18):10037–10041

Barca GM, Bertoni C, Carrington L, Datta D, De Silva N, Deustua JE, Fedorov DG, Gour JR, Gunina AO, Guidez E (2020) Recent developments in the general atomic and molecular electronic structure system. J Chem Phys 152(15):154102

Berman HM, Westbrook J, Feng Z, Gilliland G, Bhat TN, Weissig H, Shindyalov IN, Bourne PE (2000) The protein data bank. Nucleic Acids Res 28(1):235–242

Bradshaw JM, Waksman G (1998) Calorimetric investigation of proton linkage by monitoring both the enthalpy and association constant of binding: application to the interaction of the Src SH2 domain with a high-affinity tyrosyl phosphopeptide. Biochemistry 37(44):15400–15407

Brandt EG, Hellgren M, Brinck T, Bergman T, Edholm O (2009) Molecular dynamics study of zinc binding to cysteines in a peptide mimic of the alcohol dehydrogenase structural zinc site. Phys Chem Chem Phys 11(6):975–983

Bredenberg J, Nilsson L (2001) Modeling zinc sulfhydryl bonds in zinc fingers. Int J Quantum Chem 83(3–4):230–244

Brooks BR, Brooks CL III, Mackerell AD Jr, Nilsson L, Petrella RJ, Roux B, Won Y, Archontis G, Bartels C, Boresch S (2009) CHARMM: the biomolecular simulation program. J Comput Chem 30(10):1545–1614

Burrell LM, Johnston CI, Tikellis C, Cooper ME (2004) ACE2, a new regulator of the renin-angiotensin system. Trends Endocrinol Metab 15(4):166–169

Calimet N, Simonson T (2006) Cys(x)His(y)-Zn^{2+} interactions: possibilities and limitations of a simple pairwise force field. J Mol Graph Model 24(5):404–411

Case DA, Belfon K, Ben-Shalom IY, Brozell SR, Cerutti DS (2020) AMBER 2020. University of California, San Francisco

Cerdà-Costa N, Gomis-Rüth FX (2014) Architecture and function of metallopeptidase catalytic domains. Protein Sci 23(2):123–144

Chen VB, Arendall WB, Headd JJ, Keedy DA, Immormino RM, Kapral GJ, Murray LW, Richardson JS, Richardson DC (2010) MolProbity: all-atom structure validation for macromolecular crystallography. Acta Crystallogr D 66(1):12–21

Clayton D, Hanchapola I, Thomas WG, Widdop RE, Smith AI, Perlmutter P, Aguilar MI (2015) Structural determinants for binding to angiotensin converting enzyme 2 (ACE2) and angiotensin receptors 1 and 2. Front Pharmacol 6:5

Der B (2013) Computational design of zinc binding sites at protein interfaces and enzyme active sites. PhD thesis, University of North Carolina, USA

Donini OA, Kollman PA (2000) Calculation and prediction of binding free energies for the matrix metalloproteinases. J Med Chem 43(22):4180–4188

Ghorbani M, Brooks BR, Klauda JB (2020) Critical sequence hotspots for binding of novel coronavirus to angiotensin converter enzyme as evaluated by molecular simulations. J Phys Chem B 124(45):10034–10047

Glowacka I, Bertram S, Müller MA, Allen P, Soilleux E, Pfefferle S, Steffen I, Tsegaye TS, He Y, Gnirss K, Niemeyer D, Schneider H, Drosten C, Pöhlmann S (2011) Evidence that TMPRSS2 activates the severe acute respiratory syndrome coronavirus spike protein for membrane fusion and reduces viral control by the humoral immune response. J Virol 85(9):4122–4134

Gordon JC, Myers JB, Folta T, Shoja V, Heath LS, Onufriev A (2005) H++: a server for estimating p K as and adding missing hydrogens to macromolecules. Nucleic Acids Res 33(suppl_2):W368–W371

Grant BJ, Rodrigues AP, ElSawy KM, McCammon JA, Caves LS (2006) Bio3d: an R package for the comparative analysis of protein structures. Bioinformatics 22(21):2695–2696

Gresh N (1995) Energetics of Zn2+ binding to a series of biologically relevant ligands: a molecular mechanics investigation grounded on ab initio self-consistent field supermolecular computations. J Comput Chem 16(7):856–882

Han Y, Král P (2020) Computational design of ACE2-based peptide inhibitors of SARS-CoV-2. ACS Nano 14(4):5143–5147

Hoops SC, Anderson KW, Merz KM (1991) Force field design for metalloproteins. J Am Chem Soc 113(22):8262–8270

Hou T, Wang J, Li Y, Wang W (2011) Assessing the performance of the MM/PBSA and MM/GBSA methods. 1. The accuracy of binding free energy calculations based on molecular dynamics simulations. J Chem Inf Model 51(1):69–82

Humphrey W, Dalke A, Schulten K (1996) VMD: Visual molecular dynamics. J Mol Graph 14(1):33–38

Jeong W-j, Bu J, Kubiatowicz LJ, Chen SS, Kim Y, Hong S (2018) Peptide–nanoparticle conjugates: a next generation of diagnostic and therapeutic platforms? Nano Converg 5(1):1–18

Jia H (2016) Pulmonary angiotensin-converting enzyme 2 (ACE2) and inflammatory lung disease. Shock 46(3):239–248

Jo S, Kim T, Iyer VG, Im W (2008) CHARMM-GUI: a web-based graphical user interface for CHARMM. J Comput Chem 29(11):1859–1865

Jo S, Cheng X, Islam SM, Huang L, Rui H, Zhu A, Lee HS, Qi Y, Han W, Vanommeslaeghe K (2014) CHARMM-GUI PDB manipulator for advanced modeling and simulations of proteins containing nonstandard residues. Adv Protein Chem Struct Biol 96:235–265

Koca J, Zhan CG, Rittenhouse RC, Ornstein RL (2003) Coordination number of zinc ions in the phosphotriesterase active site by molecular dynamics and quantum mechanics. J Comput Chem 24(3):368–378

Kuznetsov A, Arukuusk P, Härk H, Juronen E, Ustav M, Langel Ü, Järv J (2022) ACE2 peptide fragment interaction with different S1 protein sites. Int J Pept Res Ther 28(1):7

Lee J, Cheng X, Swails JM, Yeom MS, Eastman PK, Lemkul JA, Wei S, Buckner J, Jeong JC, Qi Y (2016) CHARMM-GUI input generator for NAMD, GROMACS, AMBER, OpenMM, and CHARMM/OpenMM simulations using the CHARMM36 additive force field. J Chem Theory Comput 12(1):405–413

Li P, Merz KM Jr (2016) MCPB.py: a python based metal center parameter builder. J Chem Inf Model 56:599

Li W, Moore MJ, Vasilieva N, Sui J, Wong SK, Berne MA, Somasundaran M, Sullivan JL, Luzuriaga K, Greenough TC, Choe H, Farzan M (2003) Angiotensin-converting enzyme 2 is a functional receptor for the SARS coronavirus. Nature 426(6965):450–454

Li W, Zhang J, Wang J, Wang W (2008) Metal-coupled folding of Cys2His2 zinc-finger. J Am Chem Soc 130(3):892–900

Lin YL, Lim C (2004) Factors governing the protonation state of Zn-bound histidine in proteins: a DFT/CDM study. J Am Chem Soc 126(8):2602–2612

Lin F, Wang R (2010) Systematic derivation of AMBER force field parameters applicable to zinc-containing systems. J Chem Theory Comput 6(6):1852–1870

Liu H, Hou T (2016) CaFE: a tool for binding affinity prediction using end-point free energy methods. Bioinformatics 32(14):2216–2218

Moore GJ, Pires JM, Kelaidonis K, Gadanec LK, Zulli A, Apostolopoulos V, Matsoukas JM (2021) Receptor interactions of Angiotensin II and Angiotensin receptor blockers-relevance to COVID-19. Biomolecules 11(7):979

Myers J, Grothaus G, Narayanan S, Onufriev A (2006) A simple clustering algorithm can be accurate enough for use in calculations of pKs in macromolecules. Proteins 63(4):928–938

Padhan R, Prabheesh KP (2021) The economics of COVID-19 pandemic: a survey. Econ Anal Policy 70:220–237

Peters MB, Yang Y, Wang B, Füsti-Molnár L, Weaver MN, Merz KM Jr (2010) Structural survey of zinc containing proteins and the development of the zinc AMBER force field (ZAFF). J Chem Theory Comput 6(9):2935–2947

Phillips JC, Braun R, Wang W, Gumbart J, Tajkhorshid E, Villa E, Chipot C, Skeel RD, Kale L, Schulten K (2005) Scalable molecular dynamics with NAMD. J Comput Chem 26(16):1781–1802

Rifai EA, van Dijk M, Vermeulen NPE, Yanuar A, Geerke DP (2019) A comparative linear interaction energy and MM/PBSA study on SIRT1lLigand binding free energy calculation. J Chem Inf Model 59(9):4018–4033

Roy U (2016) Structural characterizations of the fas receptor and the fas-associated protein with death domain interactions. Protein J 35(1):51–60

Roy U (2019) 3D modeling of tumor necrosis factor receptor and tumor necrosis factor-bound receptor systems. Mol Inform 38(5):1800011

Roy U (2020a) Insight into the structures of interleukin-18 systems. Comput Biol Chem 88:107353

Roy U (2020b) Structural and molecular analyses of functional epitopes and escape mutants in Japanese encephalitis virus envelope protein domain III. Immunol Res 68(2):81–89

Santos RA (2014) Angiotensin-(1–7). Hypertension 63(6):1138–1147

Shulla A, Heald-Sargent T, Subramanya G, Zhao J, Perlman S, Gallagher T (2011) A transmembrane serine protease is linked to the severe acute respiratory syndrome coronavirus receptor and activates virus entry. J Virol 85(2):873–882

Spinello A, Saltalamacchia A, Magistrato A (2020) Is the rigidity of SARS-CoV-2 spike receptor-binding motif the hallmark for its enhanced infectivity? Insights from all-atom simulations. J Phys Chem Lett 11(12):4785–4790

Spyroulias GA, Nikolakopoulou P, Tzakos A, Gerothanassis IP, Magafa V, Manessi-Zoupa E, Cordopatis P (2003) Comparison of the solution structures of angiotensin I & II: implication for structure-function relationship. Eur J Biochem 270(10):2163–2173

Stote R, Karplus M (1995) Zinc binding in proteins and solution A simple but accurate nonbonded representation. Proteins 23(1):12–31

Sur S, Tantakitti F, Matson JB, Stupp SI (2015) Epitope topography controls bioactivity in supramolecular nanofibers. Biomater Sci 3(3):520–532

Toba S, Damodaran KV, Merz KM (1999) Binding preferences of hydroxamate Inhibitors of the matrix metalloproteinase human fibroblast collagenase. J Med Chem 42(7):1225–1234

Towler P, Staker B, Prasad SG, Menon S, Tang J, Parsons T, Ryan D, Fisher M, Williams D, Dales NA (2004) ACE2 X-ray structures reveal a large hinge-bending motion important for inhibitor binding and catalysis. J Biol Chem 279(17):17996–18007

Trzaskowski B, Adamowicz L, Deymier PA (2008) A theoretical study of zinc(II) interactions with amino acid models and peptide fragments. J Biol Inorg Chem 13(1):133–137

Vedani A, Huhta DW (1990) A new force field for modeling metalloproteins. J Am Chem Soc 112(12):4759–4767

Wang E, Weng G, Sun H, Du H, Zhu F, Chen F, Wang Z, Hou T (2019) Assessing the performance of the MM/PBSA and MM/GBSA methods. 10. Impacts of enhanced sampling and variable dielectric model on protein–protein Interactions. Phys Chem Chem Phys 21(35):18958–18969

Wang K, Lyu N, Diao H, Jin S, Zeng T, Zhou Y, Wu R (2020) GM-DockZn: a geometry matching-based docking algorithm for zinc proteins. Bioinformatics 36(13):4004–4011

Williams-Noonan BJ, Todorova N, Kulkarni K, Aguilar MI, Yarovsky I (2021) An active site inhibitor induces conformational penalties for ACE2 recognition by the spike protein of SARS-CoV-2. J Phys Chem B 125(10):2533–2550

Woo H-J, Roux B (2005) Calculation of absolute protein–ligand binding free energy from computer simulations. Proc Natl Acad Sci USA 102(19):6825–6830

Yan R, Zhang Y, Li Y, Xia L, Guo Y, Zhou Q (2020) Structural basis for the recognition of SARS-CoV-2 by full-length human ACE2. Science 367(6485):1444–1448

Yu Z, Li P, Merz KM Jr (2018) Extended zinc AMBER force field (EZAFF). J Chem Theory Comput 14(1):242–254

Zhang J, Yang W, Piquemal J-P, Ren P (2012) Modeling structural coordination and ligand binding in zinc proteins with a polarizable potential. J Chem Theory Comput 8(4):1314–1324